Paleoceanography (in press) May 17 1999

Forward modeling of carbonate proxy data from planktonic foraminifera using oxygen isotope tracers in a global ocean model

Gavin A. Schmidt
NASA Goddard Institute for Space Studies and Center for Climate Systems Research,
Columbia University, New York

Abstract

The distribution and variation of oxygen isotopes in seawater are calculated using the Goddard Institute for Space Studies global ocean model. Simple ecological models are used to estimate the planktonic foraminiferal abundance as a function of depth, column temperature, season, light intensity, and density stratification. These models are combined to forward model isotopic signals recorded in calcareous ocean sediment. The sensitivity of the results to the changes in foraminiferal ecology, secondary calcification, and dissolution are also examined. Simulated present-day isotopic values for ecology relevant for multiple species compare well with core-top data. Hindcasts of sea surface temperature and salinity are made from time series of the modeled carbonate isotope values as the model climate changes. Paleoclimatic inferences from these carbonate isotope records are strongly affected by erroneous assumptions concerning the covariations of temperature, salinity, and $\delta^{18}O_w$. Habitat-imposed biases are less important, although errors due to temperature-dependent abundances can be significant.

1. Introduction

Much of the evidence for long term variability in the oceans comes from examination of the ratio of oxygen isotopes (^{18}O to ^{16}O, expressed as an oxygen isotope composition ratio $\delta^{18}O_c$) in foraminiferal calcite deposits in ocean sediments. However, the difficulty in assigning an unambiguous climatic cause to $\delta^{18}O_c$ changes seen in a deep-sea core record is well known [*Mix*, 1987]. In order to derive a paleotemperature record from the core, assumptions concerning the variation of the ambient ratio in the seawater ($\delta^{18}O_w$) must be made. Conversely, if local temperature variations are assumed to be small or if other evidence exists to constrain them (for instance, faunal assemblages or alkenone ratios), a residual record of variations in background ratio can be derived [*Shackleton*, 1967; *Duplessy et al.*, 1991]. For benthic (bottom-dwelling) foraminifera the $\delta^{18}O_c$ signal has been interpreted as a global ice-volume record. For planktonic foraminifera, if one also assumes that linear regressions measured in today's oceans [*Craig and Gordon*, 1965; *Broecker*, 1986; *Fairbanks et al.*, 1992] of salinity S and $\delta^{18}O_w$ were valid at other times, paleosalinity records can be derived [*Duplessy et al.*, 1993; *Rostek et al.*, 1993; *Wang et al.*, 1995].

However, these interpretations must be qualified by the recognition that errors in these assumptions may bias the results. For instance, covariation of $\delta^{18}O_w$ with temperature may cause a muting or amplification of the $\delta^{18}O_c$ signal; changes in foraminiferal behavior could cause a change in depth habitat that could alias a climatic signal; changes in advection and freshwater budgets could vary the $\delta^{18}O$:S relationship [*Rohling and Bigg*, 1998].

Numerous authors have attempted to account for these effects and refine the basic assumptions [*Lohmann*, 1995; *Mix*, 1987; *Mulitza et al.*, 1998]. This paper outlines a methodology and presents preliminary results from an exercise in the forward modeling of proxy data. Forward modeling is the simulation not only of physically important prognostic variables but also of the process by which signals are recorded, in this instance, in the foraminiferal $\delta^{18}O_c$ record in deep-sea sediments (Figure 1). This methodology has the great advantage of including the physics of water isotopes as well as the ecology and population dynamics of foraminifera. Any climatic change in the model can be mapped directly to the signal recorded in the sediments. Potentially, this could lead to the refining of the patterns of spatial and temporal sedimentary changes that correspond to hypothesized meltwater pulses, thermohaline circulation variations, and eventually, full glacial cycles.

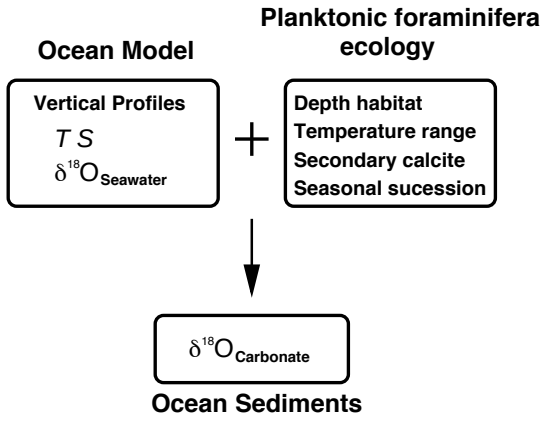

Figure 1. Outline of the forward modeling procedure. The output $\delta^{18}O_c$ can be used to verify and/or develop assumptions for interpreting proxy data. Climate changes in the ocean model can be mapped directly to the $\delta^{18}O_c$ signal that would be recorded in sediments.

The results are from experiments with the Goddard Institute for Space Studies (GISS) global ocean general circulation model (GCM), which includes oxygen isotope tracers [*Schmidt*, 1998] combined with a series of simple ecological models for calculating $\delta^{18}O_c$ in sediments. While ocean GCMs are known to have weaknesses and the ecological models used are very simple, this preliminary study simulates, for the first time, most of the major sources of uncertainty.

Since both $\delta^{18}O_w$ and environmental controls on the abundance of various species of foraminifera are allowed to vary with the changes of ocean climate in the model, any aliasing of climatic signals in the sediment can be investigated and quantified. In particular, the effect of covariations of $\delta^{18}O_w$ and temperature and the effects of vertical migration and temperature-dependent blooms on the ability to reconstruct past sea surface temperature and salinity are investigated.

The paper is split into three parts: the first part provides details of the ocean model used, the implementation of the isotope physics, and the ecological models. The second part compares model-predicted values of $\delta^{18}O_c$ with those taken from various core-tops, and finally, the last part analyzes time series of $\delta^{18}O_c$ derived from the model and assesses the reliability of standard downcore techniques to hindcast

sea surface conditions.

2. Ocean Model

The ocean model used in this study is derived from the fully coupled GISS atmosphere-ocean GCM [*Russell et al.*, 1995]. It is a mass- and tracer-conserving primitive equation model with $4^\circ \times 5^\circ$ resolution incorporating a free ocean surface, sea ice thermodynamics, and advection and a linear upstream scheme for advecting the tracers and their gradients. It differs from the model described previously [*Schmidt*, 1998] in that it now includes an explicit K-profile parameterization (KPP) ocean boundary layer scheme [*Large et al.*, 1994] and horizontal momentum diffusion [*Wajsowicz*, 1993] instead of a binomial filter. The model is initialized with climatological temperature and salinity fields [*Levitus et al.*, 1994] and sea ice mass and extent (C. Parkinson, personal communication, 1998) and uses full flux boundary conditions at the surface using seasonally varying atmospheric variables. The atmospheric fields are taken from climatology: absorbed shortwave and longwave heat fluxes [*Rossow and Zhang*, 1995]; surface air temperature, surface relative humidity, and sea level pressure [*Oort*, 1983]; and precipitation [*Legates and Willmott*, 1990]. The surface wind speed and wind stress are taken from the fully coupled model. Outgoing longwave radiation, latent and sensible heat fluxes, and evaporation are calculated prognostically. The river runoff used in the model is calculated by the land surface component of the coupled model consistent with the atmospheric fields. Once these monthly runoff values are calculated, they are fixed for the ocean run. The ocean also receives runoff from glaciers in Greenland and Antarctica, which is spread evenly around the continent. This is seasonally invariant and based on Intergovernmental Panel on Climate Change (IPCC) estimates (316×10^{12} and 2016×10^{12} kg year^{-1}, respectively) [*Houghton et al.*, 1990].

A small artificial feedback is introduced, through the surface drag coefficient used to calculate the surface freshwater flux, which controls the absolute amount of open ocean evaporation to ensure long-term mass balance. The model is run with a reduced gravity at the surface to slow down surface gravity waves and allow for a longer time step (15 min. for the dynamics and 3 hours for the source terms and tracer advection).

The full flux boundary conditions are mandated by the need to separate evaporation and precipitation in order to calculate the isotopic exchange at the surface. Any addition of an artificial salt flux in the model (such as a climatological restoring term) will affect the tracer/salinity relationship in an unphysical manner and hence must be avoided. Over the long term (> 100 years) this leads to significant drift in the ocean model (particularly in the salinity). Model deficiencies include an inability to sustain the poleward transport of salt by the Gulf Stream and North Atlantic drift, which leads to a freshening of the surface Greenland-Iceland Sea and North Atlantic. This in turn, leads to a weakening and shallowing of the North Atlantic overturning stream function. The mid-Atlantic is consequently too salty. In the equatorial region, surface waters are too fresh in the mid-Pacific; they are too warm in the Indian Ocean; and the thermocline is too diffuse. Under the Antarctic sea ice the model tends to mix down too deep. Generally, the model has a good representation of the upper ocean temperature (Plate 1). The use of the KPP boundary layer mixing scheme improved these aspects considerably over previous work with this model.

3. Isotope Tracers

The isotopic physics included in the model is mainly due to fractionation effects at changes of phase and the specification of suitable boundary conditions. The tracer used is mass of the water molecule $H_2^{18}O$ containing the water isotope. The mass of $H_2^{16}O$ in the seawater is run as a separate tracer. Isotope values are given using the standard "δ per mil" notation defined as

$$\delta^{18}\mathrm{O} = \left(\frac{R_{\mathrm{sample}}}{R_{\mathrm{standard}}} - 1 \right) \times 1000$$

where $R = \mathrm{H_2^{18}O/H_2^{16}O}$. Peedee belemnite (PDB) is used as the standard for carbonates, and Vienna standard mean ocean water (VSMOW) is used as the standard for seawater.

3.1. Fractionation Effects

At changes of phase from liquid or gas there is an associated fractionation that is either assumed to occur in equilibrium or by "kinetic fractionation" in cases where the phases are not generally in contact long enough for equilibrium to be achieved. For instance, the formation of sea ice is assumed to occur at equilibrium, i.e.,$R_i = \alpha_{wi} R_w$, where $\alpha_{wi} (> 1)$ is the liquid to ice fractionation factor and R denotes

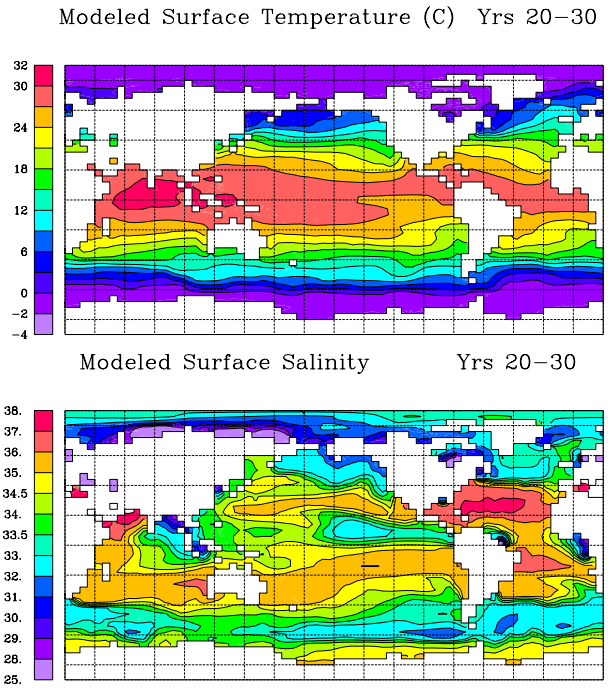

Plate 1. Surface temperature and salinity fields (10 year average) after 30 years of integration of the ocean model. The comparison with climatology is reasonable except in the vicinity of the North Atlantic where a too weak Gulf Stream leads to cooler and fresher waters. Also, the Pacific cool tongue is too fresh.

the mass ratio of the water molecules in the ice (R_i) and liquid water (R_w) phases. Similarly, α_{wv} is the liquid to vapor fractionation factor. The values and temperature dependence of these factors are outlined in Table 1. Sea ice melting and evaporation over ice are not accompanied by any fractionation.

Evaporation and condensation over open water occur with kinetic fractionation. A number of parameterizations based on a simple linear resistance model have been proposed to represent this process. All can be essentially written as

$$R_E = \frac{(\alpha_{wv} R_w - h R_a)}{(1-h)}(1-K)$$

where R_E and R_a are the isotopic ratios of the evaporating liquid and marine vapor, h is the relative humidity, and K is the kinetic fractionation parameter.

In an ocean-only model, there may be a drift in the ocean tracer mass since there is no physical mechanism to ensure that $R_{\text{precip}} \equiv R_{\text{evap}}$ globally for the annual average. Hence, in order to maintain the tracer mass balance there is an artificial control of the evaporation of tracer to achieve balance at a reasonable level. Each year, a factor controlling the amount of tracer evaporation is gently adjusted so as to keep the global annual average concentration of isotope as close as possible to mean values (VSMOW) based on the mass imbalance over the previous year. Since marine evaporation is 99.7% of the evaporation in the model, this is functionally equivalent to changing the kinetic fractionation parameter K. This clearly limits the sensitivity of the model to different formulations for K. However, two functional forms for K have been tested with this model. Primarily, a constant value, $K = 0.007$ [*Gat*, 1996], is used, and as a test of the sensitivity of the model, a wind-speed-dependent formulation based on experimental evidence [*Merlivat and Jouzel*, 1979] was used:

$$K = \begin{cases} 0.006 & V < 7 \text{ m s}^{-1} \\ 0.00082 + 0.000285V & V > 7 \text{ m}^{-1} \end{cases}$$

In the runs discussed the net average K (including the feedback) is 0.0064, and the differences in the surface ocean $\delta^{18}O_w$ seen with the different formulations are ~0.01‰.

Table 1. Isotopic Physical Constants

Fractionation Factors		Value
Water → ice (at 0°C)[a]	α_{wi}	1.003
Water → vapor[b]	α_{wv}	$0.9884 + 1.025 \times 10^{-4} T$ $-3.57 \times 10^{-7} T^2$
Vapor → ice[b]	α_{vi}	$1.015 - 1.36 \times 10^{-4} T$

The temperature-dependent formulas are linear or quadratic approximations to empirical data valid over the range 0–40°C.

[a]Average of various sources: 1.0027 [*Craig and Gordon*, 1965], 1.0029 [*Lehmann and Siegenthaler*, 1991], 1.0035 [*Majoube*, 1971], and 1.0026 [*Macdonald et al.*, 1995].

[b]From *Gat and Gonfiantini* [1981].

3.2. Isotope Boundary Conditions

The necessary boundary conditions for an ocean-only run consist of the isotopic content of freshwater coming into the oceans from precipitation, river and glacial runoff, and the isotopic composition of

the water vapor since the fractionation that occurs during evaporation is dependent upon it. These conditions can be either taken from data or from model output. Previously [*Schmidt*, 1998], the isotopic content in precipitation was set using a global regression with the local temperature and the amount of precipitation [*Gat and Gonfiantini*, 1981]. However, the data from which this regression was derived are mainly from over the continents and from some island stations. The high latitudes are particularly underrepresented, and the tropical amount effect [*Rozanski et al.*, 1993] is not well captured. Hence, for these experiments, data from an atmospheric GCM (AGCM) with water isotope tracers were used [*Jouzel et al.*, 1991]. The isotopic content of atmospheric water vapor is also taken from the AGCM results. Together, these changes significantly improve the isotopic fluxes in the Arctic and the sea surface values in the equatorial Pacific. The seasonal cycle in these boundary conditions are an important determinant of the seasonal cycle of sea surface isotope ratios. Hence the modeled seasonality may be dependent upon which AGCM results are used. This will remain an issue until fully coupled ocean-atmosphere isotopic models become available.

The amount and isotopic content of river runoff are calculated using the land surface code from the coupled GISS GCM consistent with the isotopic content of precipitation and the atmospheric climatologies [*Jouzel et al.*, 1991]. For example, modeled (observed) Arctic river runoff is 271 (275) km^3 month^{-1} and -17.9‰ (-21.0‰) [*Aagaard and Carmack*, 1989; *Östlund and Hut*, 1984], and Amazon flow is 482 (525) km^3 month^{-1}, and -6.1‰ (-3 to -5‰) [*Milliman and Meade*, 1983; *Mook*, 1982]. Other major rivers have qualitatively correct runoff and reasonable isotopic content. Meltwater from glaciers/ice caps has a fixed composition δ^{18}O= -30‰.

3.3. Initial Conditions

The ocean tracers are initialized using linearly interpolated zonal profiles in each basin taken from the deep-ocean profiles from the Geochemical Ocean Sections Study (GEOSECS) [*Östlund et al.*, 1987] combined with more recent data from the Arctic and Southern Oceans [*Bauch et al.*, 1995; *Frew et al.*, 1995]. The largest variations in $\delta^{18}O_w$ occur in the surface water; hence, whatever the surface initial condition, it equilibrates quickly (with a timescale of upper ocean mixing processes ≈10 years). Deep water characteristics do not vary as much and, apart from small distinctions between the main water masses (North Atlantic Deep Water, Antarctic Bottom Water, and Deep Pacific and Indian Water), are relatively homogeneous. Sea ice is initially assumed to be in isotopic equilibrium with the local surface water, and again, this takes a few years to equilibrate.

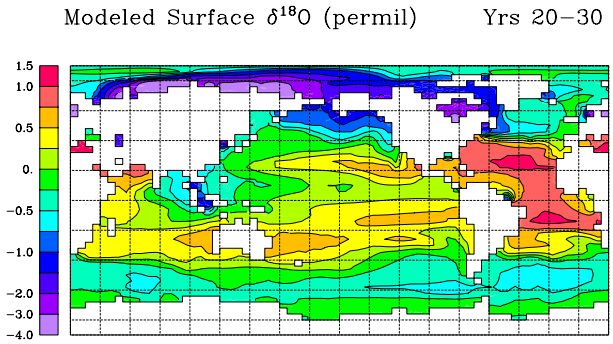

Plate 2. Surface $\delta^{18}O_w$ field (10 year average) after 30 years of integration of the ocean model. The comparison to the relatively sparse observations is good everywhere except in the North Atlantic region and the mid-Pacific.

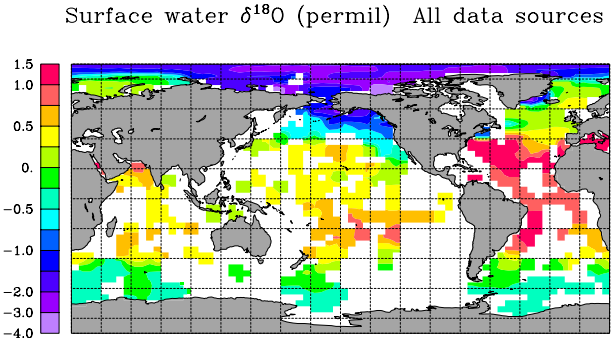

Plate 3. Amalgamated observations of open ocean $\delta^{18}O_w$ taken from Geochemical Ocean Sections Study (GEOSECS), and other sources [*Epstein and Mayeda*, 1953; *Craig and Gordon*, 1965; *Weiss et al.*, 1979; *Duplessy et al.*, 1981; *Östlund and Hut*, 1984; *Ganssen and Kroon*, 1991; *Macdonald et al.*, 1995; *Bauch et al.*, 1995; *Frew et al.*, 1995; *Wellington et al.*, 1996; *Cooper et al.*, 1997; *Archambeau et al.*, 1998, H. Craig, unpublished data, 1987; K. J. Heywood, unpublished data, 1993; A. Juillet-Leclerc, unpublished data, 1998; G. Gannsen, unpublished data, 1988; J.-C. Duplessy, unpublished data, 1998]. The data were interpolated onto a 4° × 5° grid. Gaps indicate that no data was found within 5° of that box. No attempt has been made to correct for seasonal effects.

3.4. Comparison With Observations

Plate 2 shows the 10 year average modeled δ^{18}O of surface seawater after 30 years integration. The general pattern is robust: high values in the subtropics (particularly in the Atlantic) with more depleted values in the subpolar regions and equatorial Pacific. Note that values in the North Atlantic are slightly depleted relative to observations (Plate 3) in a similar manner to the salinity (Plate 1) because of a weak North Atlantic drift in the model. Observed regional linear relationships between salinity and $\delta^{18}O_w$ are well captured by the model. Comparison with the GEOSECS data (Figure 2) shows the modeled relationship in the Atlantic and Pacific is very similar to that seen in observations. There is a departure from the observations for relatively fresh samples in the Atlantic because of the slightly heavier than observed Arctic freshwater end member. Southern Ocean model output and data are similarly close (not shown). Despite this good agreement over limited regions, data taken from the entire open ocean (Figure 3) show a clear distinction between the tropics and extratropics and a large amount of scatter around the linear regressions.

Another important feature in the modeled results that is not clear in the observations are the large zonal gradients in $\delta^{18}O_w$ at the latitudes of the subtropical gyres. These differences arise because of both advective processes and latitudinally varying evaporation/precipitation fields and hence highlight the need for a dynamic global ocean model to account for these effects.

4. Ecological Models

The actual growth of foraminifera in the ocean is a complicated process depending on availability of nutrients, light intensity (for symbiotic species), temperature, stratification, and ocean dynamics. The isotopic content of the calcite shell is generally close to being in equilibrium with the surroundings but can be affected by various disequilibrium effects (that depend, for example, on dissolved bicarbonate concentrations [*Spero et al.*, 1997] or the photosynthetic activity of algal symbiontes [*Bemis et al.*, 1998]). This study is concerned with assessing the first-order effects of changing thermocline depths and temperature tolerances on the recorded isotopic signal. Hence calcite is always assumed to precipitate in equilibrium [*Kim and O'Neil*, 1997].

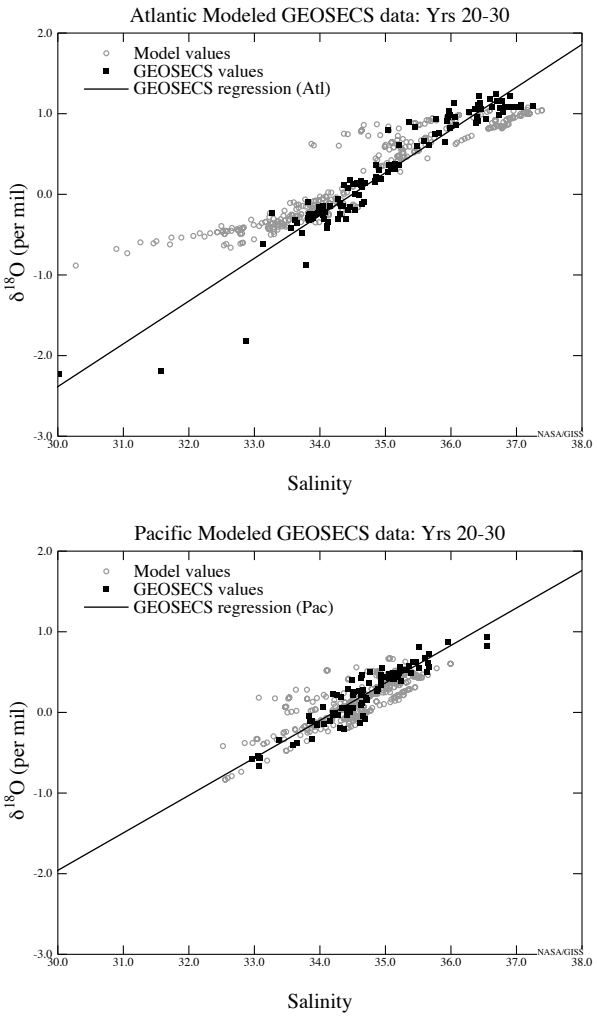

Figure 2. Comparison of the relationship between salinity and surface $\delta^{18}O_w$ found in the GEOSECS Atlantic and Pacific sections (above 250 m depth) and the model output. The model results are drawn from 10 year average fields after 30 years of integration at the sites in the model closest to the GEOSECS stations.

At specific sites in the GCM, monthly values of the prognostic variables (temperature, salinity, $\delta^{18}O_w$, and mixed layer depth) are stored for the vertical water column. Equilibrium calcite values are then calculated at every depth and through time. The ecological model then weights the calculated $\delta^{18}O_c$ values in the vertical and by month. This procedure gives a $\delta^{18}O_c$ value in the sediments that is typical for the average sediment deposited that year.

The models used are very simple but, nonetheless, span a wide range of possible foraminiferal responses. Each model is essentially a different way to weight

the equilibrium calcite with depth and through time roughly based on presumed foraminiferal abundance. The main interest is in the correlation between important climatic variables (sea surface temperatures and salinities) and changes to these weighting functions. The models must make three basic assumptions: the water depth(s) at which (planktonic) foraminifera live (accrete carbonate), their seasonal growth patterns, and local environmental limits on their growth. Precipitation of the carbonate is assumed to be contemporaneous with foraminiferal abundance. A calculation of the amount of carbonate flux would necessarily involve a carbon and nutrient cycle model and would add enormously to the complexity of these experiments. Fortunately, the isotopic composition of the carbonate sediment is generally assumed to be independent of accumulation rate.

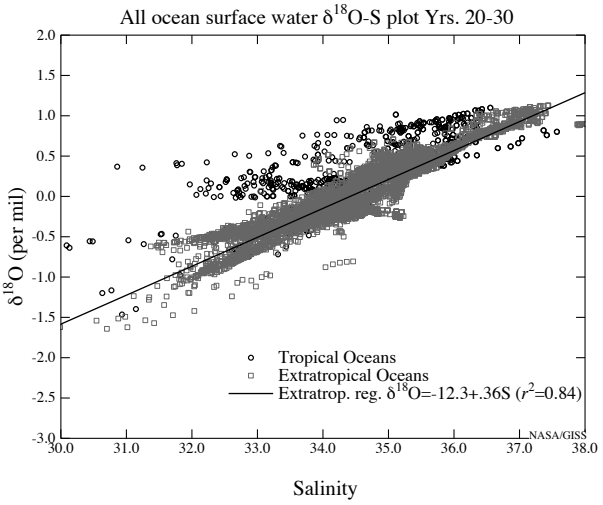

Figure 3. Comparison of the relationship between salinity and $\delta^{18}O_w$ in surface (<30 m) modeled output from all open ocean points (not including the Arctic). Note that the tropical surface waters follow a distinct pattern separate from that seen in the extratropics. The linear regression for the extratropics is more shallow than that seen in the observations (slope of 0.36 compared to 0.5).

The ecological models are applied to monthly depth profiles taken from a single year (year 23) of the model run. Upper ocean values have adjusted by then, and the model is relatively stable. The largest departure from climatology in surface salinity (and isotopic values) is in the North Atlantic where salinity is up to 2 too low and $\delta^{18}O_w$ is $\sim$0.6‰ too low. Using longer averages or different years does not markedly change the results.

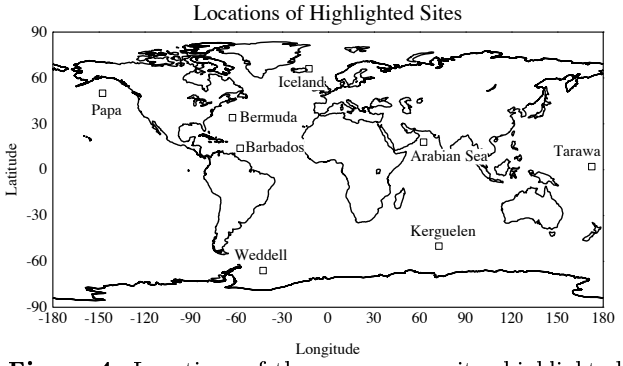

Figure 4. Locations of the open ocean sites highlighted in the text: Iceland, Bermuda, Barbados, Tarawa, Kerguelen, Papa, Arabian Sea, and Weddell. Details can be found in Table 2.

The profiles are taken from a number of different sites that characterize a variety of open ocean environments (Figure 4). Annual average profiles of T, S, and $\delta^{18}O_w$ for these sites are shown in Figure 5. The isotope profiles are generally in line with the observations, although general biases can be seen in the profiles. Notably, there is a deeper thermocline than observed at the tropical sites and the upper ocean in the North Atlantic is significantly fresher (and more depleted). Despite differences in detail from the climatologies the following experiments should serve to illustrate the consequences for the mean $\delta^{18}O_c$ of the uncertainty associated with foraminiferal ecology.

4.1. Depth of Average Growth

There are clear differences in environmental conditions (local temperature and $\delta^{18}O_w$) over depth ($\approx$0–500 m), and so, the $\delta^{18}O_c$ of each foraminifera will depend on the depth at which it accretes carbonate. Four cases are examined: equilibrium calcite at (1) a constant depth of 6 m (surface), (2) a constant depth of 45 m, (3) the average mixed layer (ML) value (where the ML depth is defined as the depth at which the potential density difference from the surface is 0.125 kg m^{-3}), and (4) the value at the deep chlorophyll maximum (DCM, defined as the stability maximum in the photic zone (top 80 m) [*Fairbanks and Wiebe*, 1980]). The mean surface carbonate values vary substantially (from 3.7‰ at Weddell to -2.7‰ at Tarawa) over the sites chosen, but some general patterns are seen. The carbonate values at the surface and in the mixed layer are very close everywhere, irrespective of the depth of the mixed layer. The DCM value is up to 0.7‰ higher than the mixed layer value.

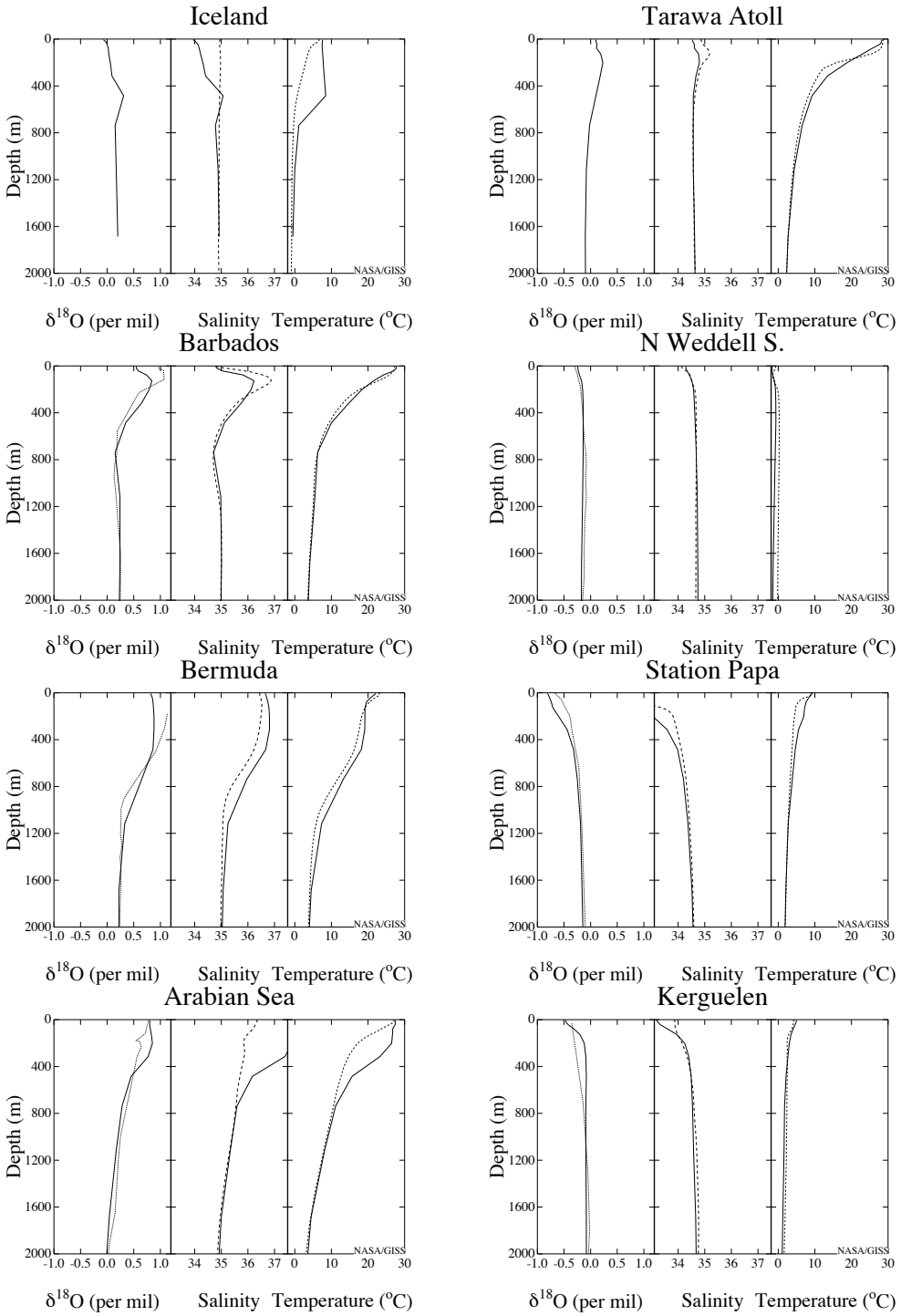

Figure 5. Annual average temperature, salinity and $\delta^{18}O_w$ depth profiles (top 2000 m, solid lines) at eight selected open ocean sites: Iceland, Bermuda, Barbados, Tarawa, Kerguelen, Papa, Arabian Sea, and Weddell. Relevant comparisons from the Levitus data set for temperature and salinity and nearby stations for $\delta^{18}O_w$ [*Östlund et al.*, 1987; *Frew et al.*, 1995] are included for comparison (dashed lines).

Except where there are deep mixed layers (Weddell, Bermuda, and Tarawa), the difference between 45 m and the surface ranges from 0.2 to 0.4‰ higher at 45 m. This is mainly due to the steep drop in temperature with depth rather than changes in $\delta^{18}O_w$, which are of relatively minor importance (< 0.05‰).

4.2. Seasonal Succession

In the middle to high latitudes there is a well-defined seasonal succession of planktonic species, with peaks of individual species occurring at different parts of the year [*Sautter and Thunell*, 1989]. Seasonal biases in $\delta^{18}O_c$ are tested by assuming that the average accretion of carbonate is weighted by the abundance of the species at a particular month. I assume that a spring bloom is weighted by month so that March, April, May, and June represent 10, 35, 40, and 15%, respectively. This implies that 35% of the carbonate deposited will reflect April conditions. The summer bloom is weighted so that May, June, July, and August represent 15, 30, 30, and 25%, respectively. For Southern Hemisphere sites, equivalent seasons are used.

At the Iceland site the ML calcite values for no seasonal cycle, spring bloom, and summer bloom are 1.56, 1.69, and 1.40‰, respectively. Again, these differences arise mostly because of the seasonal cycle of temperature and not $\delta^{18}O_w$. (Globally, the seasonal cycle in $\delta^{18}O_w$ ranges from 0 to 0.7‰. The largest amplitudes occur near river outflows and in sea ice regions.) At Papa a similar pattern is found with values of 0.48, 0.98, and 0.18‰, respectively, indicating that different seasonal growth patterns might influence $\delta^{18}O_c$ by up to 0.8‰ in the middle to high latitudes. In the Weddell Sea region, temperature changes are minimal and little difference is found. At Kerguelen the values are 1.80, 1.81, and 1.52‰, respectively.

4.3. Local Environmental Limits to Growth

Temperature and nutrient controls on foraminifera growth are probably more robust indicators of abundance since there is a wide variation in the season of maximum abundance [*Kohfeld et al.*, 1996]. Most species have a relatively well defined temperature and salinity range over which they grow optimally [*Bijma et al.*, 1990], although salinity is not a first-order constraint on growth in the open ocean. If temperatures or salinities exceed those limits, growth may be reduced or halted altogether, and subsequent environmental changes may not be recorded. Hence, I assume that if the temperature goes beyond a tolerable range, no $\delta^{18}O_c$ is recorded (i.e., the weighting for this period is zero) and that the abundance is greater near the optimal temperature [*Mix*, 1987] (assumed here to be at the center of the possible range).

In the middle to high latitudes, for instance, a cold water species might have temperature limits of −2°–9°C (denoted CO), while a warm water species might have limits of 5°–18°C (denoted WA). ML calcite values at Iceland (seasonal temperature range 6°–9°C), assuming no environmental controls (equal weighting throughout the year), CO limits, or WA limits are 1.56, 1.63, and 1.52‰, respectively. At Papa (6°–12°C) the values are 0.48, 1.00, (CO), and 0.26‰ (WA). Unsurprisingly, cold-water-preferring foraminifera give generally higher mean $\delta^{18}O_c$ values at the same site than foraminifera that prefer warmer waters. At Kerguelen (3°–6°C) the difference between CO and WA is ∼0.3‰.

In the low latitudes, temperature limits more suited to tropical species (14°–32°C) are used. Another important environmental factor that is important for symbiotic species is light intensity. This moderates both the abundance of the foraminifera and their calcification rate, which in some species at least (*Orbulina universa*, for instance), leads to isotopic disequilibrium effects [*Bemis et al.*, 1998]. I parameterize light intensity effects by assuming that abundance is related to the square of the absorbed solar radiation (the effect on isotopic disequilibrium is neglected). At all the tropical points chosen the values for no environmental controls, temperature-controlled abundance, and light-controlled abundance vary by only ∼0.1‰. This indicates the relatively weak seasonal cycles in these areas. However, more restrictive temperature limits or a higher sensitivity to light levels could increase the differences.

4.4. Secondary Calcification and Selective Dissolution

Secondary calcification can occur for some species (e.g., *Neogloboquadrina pachyderma* (l) and *Globigerinoides sacculifer*) deeper in the water column [*Lohmann*, 1995; *Kohfeld et al.*, 1996; *Bemis et al.*, 1998]. This can be easily modeled by combining ML carbonate with carbonate from the deep thermocline or at the level of the sediments. In some species (such as *N. pachyderma* (l)) the encrustation at depth can be as much as 75% of the individual's mass [*Kohfeld et al.*, 1996], although in other species the encrustation is less (∼30% for *G. sacculifer*). Selective dissolution

has been hypothesized to preferentially remove primary calcite [*Lohmann*, 1995] and that can also be modeled by changing the percentages of secondary calcite.

Differences in $\delta^{18}O_c$ for secondary calcite accreted between the mixed layer and 500 m and the ML value range from 0.5‰ higher (midlatitudes) to 2.5‰ higher (tropics). Hence, for every 10% amount of secondary calcite included the $\delta^{18}O_c$ value will increase by between 0.05 and 0.25‰. The potential for low-temperature biases is greater in the tropics (where temperature and $\delta^{18}O_w$ contrasts with depth are greater).

5. Comparison to Core-Top Data

Table 2 shows a collection of core-top isotopic measurements of *N. pachyderma* (l) from the mid-to-high latitudes and *G. sacculifer* and *Globigerinoides ruber* (white) from the tropics for comparison with the predicted values of $\delta^{18}O_c$ at similar sites in the model. The cores are within the general area of the model sites (except for the Weddell site, where the nearest cores are significantly to the east) and could be expected to reflect regional characteristics. There is a significant scatter in the field data for cores within the same region, indicating a sensitivity to small-scale regional effects, reworkings of the sediment, or the heterogeneous methods used for estimating the core-top values. The coarse resolution of the model ($4^\circ \times 5^\circ$), the errors in the physical climatology (Figure 5), and the exclusion of known disequilibrium effects preclude exact reproduction by the model of the observations, but the grosser features of the global variability should be captured. Two temperature equations are used [*Kim and O'Neil*, 1997; *Erez and Luz*, 1983] (henceforth KO97 and EL83) to highlight the uncertainty (particularly at low temperatures) in estimating equilibrium calcite.

The foraminifera chosen reflect species that have often been used for paleoclimatic reconstructions. Their estimated ecological profiles are outlined in Table 3 and are reasonable approximations to the life cycle and depth habitat of each species. There is an amount of uncertainty associated with each characteristic, although results from section 4 can be used to quantify the effect of different choices. Another commonly used species is *Globigerinoides bulloides*. However, this species is known to have substantial size and carbonate-ion-concentration-related disequilibrium effects [*Bemis et al.*, 1998], which complicate global core-top comparisons. No consistent ecological profile was found that could reasonably match the observations.

A summary of the results in this section is outlined in Table 4. For *N. pachyderma* (l) the model-predicted values using KO97 are slightly low, possibly because of lower than observed $\delta^{18}O_w$ at the Iceland site and/or incorrect specification of the depth of accretion of the secondary calcite. Interestingly, using the temperature equation from EL83, the $\delta^{18}O_c$ values are ∼0.2‰ larger and significantly closer to observations (standard error 0.33 versus 0.46‰).

Comparisons with core-tops containing *G. sacculifer* or *G. ruber* (white) are complicated by interactions with their symbionts which have been shown to lead to the incorporation of isotopically light metabolic carbonate in the shells. In the absence of a clear measure of this "vital effect," I still assume that the foraminifera precipitates in equilibrium. Given the scatter of the measurements, the predicted values are very reasonable. The differences between the temperature equations are less important, and the standard errors for both sets of results are ∼0.2‰.

In summary, the core-top comparisons for mixed layer tropical species are very good, generally within 1σ of the observed values. The underestimation of *G. sacculifer* values at the Tarawa site could be due to the very low sedimentation rate at these cores and/or the possible contamination of the core-top carbonate with heavier, glacial age sediment. Possibly, selective dissolution could have increased the percentage of secondary calcite in the deeper cores (the depths for the three core-tops in Table 2 are 3.2, 1.7, and 3.9 km, respectively). At the higher latitudes, *N. pachyderma* (l) results are reasonable. Despite flaws these profiles do a fair job of simulating the spatial variability of the $\delta^{18}O_c$ field. The effect of these profiles on temporal changes can only be tested by examining time series of $\delta^{18}O_c$ and comparing the derived isotopic temperatures and/or salinities to the actual climatic variables. This is done in the following section.

Table 2. Summary of Relevant Core-Top Data

Model Site	Core	Ref.	Lat.	Lon.	Species	$\delta^{18}O_c$
Iceland (66°N, 12.5°W)	23 246-2	D91	69.38°N	12.92°W	*N. pachyderma* (l)	3.82
	V28-56	B86	68.0°N	6.1°W	*N. pachyderma* (l)	2.8
	CH77-07	D77	66.60°N	10.52°W	*N. pachyderma* (l)	3.76[a]
	V27-38	DZ81	61.37°N	11.48°W	*N. pachyderma* (l)	3.50
Papa (50°N, 147.5°W)	PAR-87A	Z91	54.4°N	149.0°W	*N. pachyderma* (l)	2.34
Bermuda (34°N, 62.5°W)	BC-004A	K96	33.71°N	57.63°W	*G. ruber* (white)	−0.51[b]
	BC-004D				*G. ruber* (white)	−0.41[b]
	GIA	W81	32.25°N	64.00°W	*G. ruber* (white)	−0.63– −0.79[c]
Arabian Sea (18°N, 62.5°E)	A15-596	C81	18.93°N	61.38°E	*G. ruber* (white)	−1.80
	MD13-68	D81	20.68°N	60.57°E	*G. ruber* (white)	−1.66
					G. sacculifer	−1.48
	RC9-161	C81	19.57°N	59.60°E	*G. ruber* (white)	−1.61
	MD13-67	D81	19.22°N	60.67°E	*G. ruber* (white)	−1.95
					G. sacculifer	−1.25
Barbados (14°N, 57.5°W)	V26-117	DZ81	16.9°N	63.47°W	*G. ruber* (white)	−1.76
					G. sacculifer	−1.92
	V26-115	DZ81	15.85°N	62.43°W	*G. ruber* (white)	−1.99
					G. sacculifer	−1.79
Tarawa (2°N, 172.5°E)	V28-203	B86	1.0°N	179.4°W	*G. sacculifer*	−1.7
	V28-238	B86	1.0°N	160.3°E	*G. sacculifer*	−2.3
	ERDC-128	B86	0.0°	161.4°E	*G. sacculifer*	−1.8
Kerguelen (50°S, 72.5°E)	MD80-304	D91	51.07°S	67.73°E	*N. pachyderma* (l)	2.83
	MD84-560	D91	53.12°S	72.17°E	*N. pachyderma* (l)	2.43
	MD84-552	D91	54.92°S	75.83°E	*N. pachyderma* (l)	3.15
	MD84-551	D91	55.00°S	73.28°E	*N. pachyderma* (l)	3.15
Weddell (66°S, 42.5°W)	PS1 387	D91	68.73°S	5.87°W	*N. pachyderma* (l)	3.59
	PS1 431	D91	69.82°S	6.58°W	*N. pachyderma* (l)	3.46
	PS1 394	D91	70.1°S	6.85°W	*N. pachyderma* (l)	3.4

References are denoted by D91, *Duplessy et al.* [1991]; DZ81, *Durazzi* [1981]; Z91, *Zahn et al.* [1991]; W95, *Wang et al.* [1995]; W81, *Williams et al.* [1981]; C81, *Curry and Matthews* [1981]; D81, *Duplessy et al.* [1981]; B86, *Broecker* [1986]; K96, *Keigwin* [1996]; and D77, J.-C. Duplessy (unpublished data archived at the World Data Center-A for Paleoclimatology, Boulder, Colorado. http://www.ngdc.noaa.gov). *N. pachyderma* (l) is *Neogloboquadrina pachyderma* (l); *G. ruber* (white) is *Globigerinoides ruber* (white); *G. sacculifer* is *Globigerinoides sacculifer*.

[a]Estimated Holocene value.

[b]Average of all values with ages younger than 2000 yr B.P. (radiocarbon age).

[c]Range over different size fractions.

Table 3. Definition of Ecological Profiles

Profile	Species	Depth Habitat	Secondary Calcification		Temperature Range, °C	Optimum Temperature, °C
			Fraction %	Depth Range, m		
NP	*N. pachyderma* (l)	PYC	75	PYC–1300	–2–9	5.5
GR	*G. ruber* (white)	ML	0	–	14–32	23.0
GS	*G. sacculifer*	ML	30	PYC	14–32	26.5
WA	–	ML	0	-	5–18	11.5

Abundance is at a maximum at the optimum temperature (usually the mid-point of the temperature range), and decreases linearly to the limits; PYC denotes the pycnocline (maximum gradient in density); ML denotes the surface mixed layer.

Table 4. Model-Predicted Core-Top Data

Model Site	Species	Model $\delta^{18}O_c$		Mean Observation
		KO97[a]	EL83[b]	$\delta^{18}O_c$,[c]
Iceland	*N. pachyderma* (l)	2.64	2.86	3.47 ± 0.47
Papa	*N. pachyderma* (l)	2.00	2.24	2.34 ± 0.10[d]
Bermuda	*G. ruber* (white)	−0.75	−0.57	-0.59 ± 0.16
Arabian Sea	*G. ruber* (white)	−1.79	−1.67	-1.76 ± 0.15
	G. sacculifer	−1.59	−1.46	-1.37 ± 0.16
Barbados	*G. ruber* (white)	−2.05	−1.94	-1.88 ± 0.16
	G. sacculifer	−1.85	−1.73	-1.86 ± 0.09
Tarawa	*G. sacculifer*	−2.41	−2.30	-1.93 ± 0.32
Kerguelen	*N. pachyderma* (l)	2.67	2.88	2.89 ± 0.34
Weddell	*N. pachyderma* (l)	3.55	3.70	3.48 ± 0.10

Model-predicted values are calculated using the the ecological profiles outlined in Table 3, the model-generated monthly vertical profiles of T, S, and $\delta^{18}O_w$, and two different temperature equations.

[a]Calculated using $T = 16.1 - 4.64(\delta_c - \delta_w) + 0.09(\delta_c - \delta_w)^2$ [*Kim and O'Neil*, 1997] and an offset of 0.27‰ from Vienna standard mean ocean water (VSMOW) to Peedee belemnite (PDB) [*Bemis et al.*, 1998].

[b]Calculated using $T = 17.0 - 4.52(\delta_c - \delta_w) + 0.03(\delta_c - \delta_w)^2$ [*Erez and Luz*, 1983] and an offset of 0.22‰ from VSMOW to PDB [*Bemis et al.*, 1998].

[c]Averaged observations are calculated over all core-tops from Table 2. Error bars are 1σ.

[d]Error bars are taken from *Zahn et al.* [1991].

6. Hindcasts of Temperature and Salinity

There are large changes in ocean sea surface conditions for the midlatitude Iceland site as the model proceeds. The major ocean circulation change is a gradual weakening of the North Atlantic overturning stream function, which seems to be due mainly to a weak Gulf Stream and North Atlantic drift. This reduces the salinity in the North Atlantic and Greenland Sea areas and thus inhibits deep convection. The stream function falls from 18 Sv over the first decade of the run to 5 Sv over years 100–110. The consequent changes in the tracer fields over this period are substantial. While these changes do not represent any particular period or event, the sensitivity of $\delta^{18}O_c$ and the derived paleoclimatic variables to these changes are instructive and are possibly indicative of what may be expected with a rapid change of the overturning stream function in the real ocean. Most importantly, the variations in the tracer fields (isotopes, salinity, and temperature) are all physically consistent.

The *N. pachyderma* (l) (NP) ecological profile (Table 3) is used to construct a time series of $\delta^{18}O_c$ for years 10–120 of the run. In addition, the time series of annual average ML carbonate and ML carbonate with WA temperature limits (5°–18°C) are used. In an analogous procedure to that used for actual downcore data, sea surface variability is derived from these $\delta^{18}O_c$ records. First, $\delta^{18}O_w$ is assumed to have remained constant, and isotopic temperatures are calculated. Second, an isotopic salinity record is derived assuming that the exact sea surface temperature record is known from other sources and that the temporal $\delta^{18}O_w$:S gradient is equal to the extratropical spatial gradient. The derived proxy temperature and salinity records are then calibrated to the sea surface conditions at end of the model simulation (year 120) using a corrective offset (so that the "core-top" values match conditions at the end of the simulation). The differences between these proxy records and the actual sea surface conditions going back through the simulation are a measure of the sensitivity of the proxies to uncertainties in $\delta^{18}O_w$ and ecology. Additional sources of error due to systematic inaccuracies in the use of other proxy data for temperature, for example, although important, are neglected [*Schmidt*, 1999]. The differences due to the different temperature equations are minimized by the calibration, and so, only the KO97 equation is used subsequently.

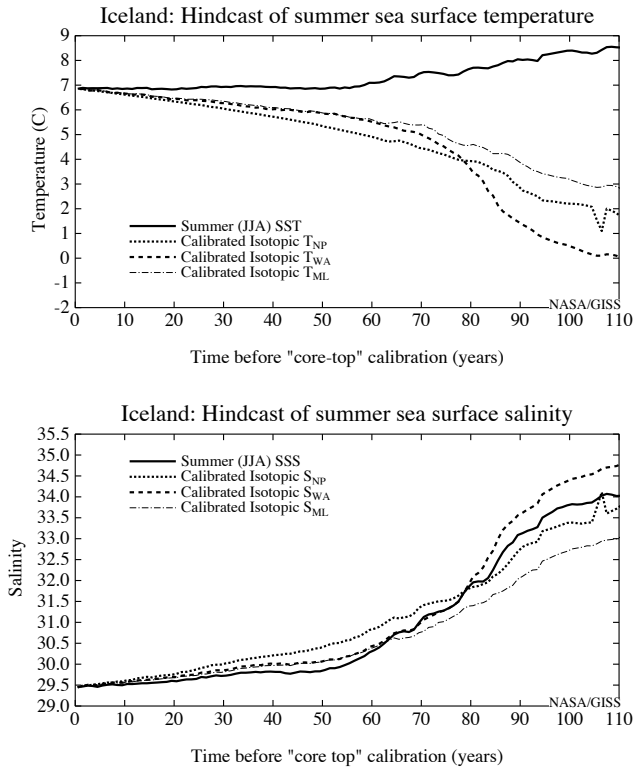

Figure 6. Hindcasts of sea surface temperature and salinity based on standard downcore analysis of the modeled $\delta^{18}O_c$ record at the Iceland site. This is where the largest changes in the model occur as North Atlantic Deep Water production slows down. All isotopic estimates are calibrated so that the last core-top value is equal to the summer surface value. Three isotopic estimates are made using $\delta^{18}O_c$ derived from the *N. pachyderma* (l) (NP) profile, the warm temperature limit (WA) profile, and the mixed layer (ML) value.

The Iceland point is highlighted since it has both large temperature and $\delta^{18}O_w$ changes over the period considered. Over the 110 year period, annual average $\delta^{18}O_w$ drops ~1.5‰, while temperature decreases ~2°C. The differences between the $\delta^{18}O_c$ records for the three profiles used (NP, WA, and ML) varies through time (NP is ~0.9‰ heavier and WA 0–0.5‰ lighter than the ML $\delta^{18}O_c$). Isotopic temperatures (Figure 6) are compromised by large variations in $\delta^{18}O_w$ and the in-phase covariation between $\delta^{18}O_w$ and T. There is an average of 0.8°C difference between the isotopic temperatures calculated from NP and WA after calibration, and both have maximum errors from summer sea surface temperature (SST) of over 7°C (at year 10).

How much of these errors are due to the variation in $\delta^{18}O_w$ compared to the ecological effects? Looking at ML, the errors are noticeably lower than those for NP or WA. This implies that while the variations in $\delta^{18}O_w$ are the main source of error in this example, the errors are compounded by the (temperature sensitive) ecology of the foraminifera.

Isotopic salinities are calculated using the exact summer SST and assuming that the temporal $\delta^{18}O_w$:S gradient is 0.36 (Figure 3). The standard error of the isotopic salinities is ∼0.35 (for NP and WA) and ∼0.5 (for ML). Maximum errors range from ∼0.6 to 1.0. In the model the temporal gradient in $\delta^{18}O_w$:S varies substantially (for changes in $\delta^{18}O_w$ greater than 0.2‰ over 100 years, the temporal gradient is $\sim 0.5 \pm 0.4$), and at a significant number of sites it is actually negative [*Schmidt*, 1999]. However, at this site the temporal gradient is ∼0.35, very close to the extratropical spatial gradient. The errors in this example come mainly from an increase in the seasonal cycle of temperature from ∼2°to ∼7°C. Since the NP profile is least affected by surface seasonality, that hindcast comes closest to the actual salinity. The WA profile overestimates changes in salinity because the temperature limits cause a shift in maximum abundance toward midsummer.

This experiment clearly does not include any atmospheric feedbacks, such as changes in surface air temperatures, precipitation, etc., that could alter the temperature/salinity/isotope profiles in addition to that caused by the mainly advective change seen here. Also, it should be stressed that the errors are due to the variations of $\delta^{18}O_w$ and the integrating effects of the ecological profiles chosen. Errors associated with using an inaccurate paleotemperature equation or possible biases in the proxy temperature used to calculate the isotopic salinities are bypassed in this experiment, although they remain important in actual applications.

7. Conclusions

The main influences on actual downcore planktonic $\delta^{18}O_c$ data are (in rough order of importance) the local temperature, ice volume changes, variations in $\delta^{18}O_w$ (the water mass effect), biological vital effects, possible ecological or behavioral changes, and selective dissolution [*Berger and Gardner*, 1975]. This paper presents a new methodology that has the potential for quantifying the effects of many of these uncertainties.

The significant spatial variations of surface $\delta^{18}O_w$ seen in the relatively sparse observations can be captured by the ocean model used here. Importantly, the modeled $\delta^{18}O_w$ covaries with temperature, for instance, in frontal regions such as the North Atlantic. Temporal covariations with salinity are not as straightforward as observed linear regressions might imply. Less certain are the results from the simple ecological models used. Predicted $\delta^{18}O_c$ for different ecological profiles and species compares well with relevant core-top data, but the effects of these profiles on the calibrated temperature or salinity reconstructions are small. This indicates that ecological variations may indeed be of second-order importance, although further work with more sophisticated nutrient cycle/ecological models is needed. As these more complicated ecological models arise, they will be relatively simple to incorporate into this framework and will allow a better assessment of potential ecological distortions.

The next stage in using these tools is to apply them to controlled climatic changes and to follow those changes through to the sediment record. Of particular interest are the response of the ocean model to meltwater pulses consistent with those of the last deglaciation and the ocean circulation at the Last Glacial Maximum (LGM). The variability of $\delta^{18}O_c$ due to the meltwater pulses might allow us to assess the degree to which cooling associated with depleted freshwater input might be disguised in the sediments. The predicted LGM distribution of $\delta^{18}O_w$ and $\delta^{18}O_c$ may be useful in addressing the LGM tropical sea surface temperature controversy and for refining the estimates of the glacial ice volume effect.

Acknowledgments. I'd like to thank D. Rind, J. Ortiz, and G. Bilodeau for interesting discussions concerning this work and G. Russell for all his help with the GISS model. The comments of D. Andreasen, J. Cole, M. Delaney, and an anonymous reviewer were particularly helpful in improving this manuscript. This work was done with the support of a NOAA Postdoctoral Fellowship in Climate and Global Change administered by the UCAR Visiting Scientist Program.

References

Aagaard, K., and E. C. Carmack, The role of sea ice and other fresh water in the Arctic circulation, *J. Geophys. Res.*, *94*, 14,485–14,498, 1989.

Archambeau, A.-S., C. Pierre, A. Poisson, and B. Schauer, Distributions of oxygen and carbon stable isotopes and CFC-12 in the water masses of the Southern Ocean at

30°E from South Africa to Antarctica: Results of the CIVA1 cruise, *J. Mar. Syst.*, *17*, 25–38, 1998.

Bauch, D., P. Schlosser, and R. G. Fairbanks, Freshwater balance and the sources of deep and bottom waters in the Arctic Ocean inferred from the distribution of $H_2^{18}O$, *Prog. Oceanogr.*, *35*, 53–80, 1995.

Bemis, B. E., H. J. Spero, J. Bijma, and D. W. Lea, Reevaluation of the oxygen isotopic composition of planktonic foraminifera: Experimental results and revised paleotemperature equations, *Paleoceanography*, *13*, 150–160, 1998.

Berger, W. H., and J. V. Gardner, On the determination of Pleistocene temperatures from planktonic foraminifera, *J. Foraminiferal Res.*, *5*, 102–113, 1975.

Bijma, J., W. W. Faber, and C. Hemleben, Temperature and salinity limits for growth and survival of some planktonic foraminfers in laboratory cultures, *J. Foraminiferal Res.*, *20*, 95–116, 1990.

Broecker, W. S., Oxygen isotope constraints on surface ocean temperatures, *Quat. Res.*, *26*, 121–134, 1986.

Cooper, L. W., T. E. Whitledge, J. M. Grebmeier, and T. Weingartner, The nutrient, salinity and stable oxygen isotope composition of Bering and Chukchi Seas waters in and near the Bering Strait, *J. Geophys. Res.*, *102*, 12,563–12,573, 1997.

Craig, H., and L. I. Gordon, Deuterium and oxygen 18 variations in the ocean and the marine atmosphere, in *Stable Isotopes in Oceanographic Studies and Paleotemperatures*, edited by E. Tongiorgi, pp. 9–130, Cons. Naz. di Rech., Spoleto, Italy, 1965.

Curry, W. B., and R. K. Matthews, Paleo-oceanographic utility of oxygen isotopic measurements on planktic foraminifera: Indian Ocean core-top evidence, *Palaeogeogr. Palaeoclimatol. Palaeoecol.*, *33*, 173–191, 1981.

Duplessy, J.-C., A. W. H. Bé, and P. L. Blanc, Oxygen and carbon isotopic composition and biogeographic distribution of planktonic foraminifera in the Indian Ocean, *Palaeogeogr. Palaeoclimatol. Palaeoecol.*, *33*, 9–46, 1981.

Duplessy, J.-C., L. Labeyrie, A. Juillet-Leclerc, F. Maitre, J. Duprat, and M. Sarnthein, Surface salinity reconstruction of the North Atlantic Ocean during the Last Glacial Maximum, *Oceanol. Acta*, *14*, 311–324, 1991.

Duplessy, J.-C., E. Bard, L. Labeyrie, J. Duprat, and J. Moyes, Oxygen isotope records and salinity changes in the Northeastern Atlantic Ocean during the last 18,000 years, *Paleoceanography*, *8*, 341–350, 1993.

Durazzi, J. T., Stable isotope studies of planktonic foraminifera in North Atlantic core tops, *Palaeogeogr. Palaeoclimatol. Palaeoecol.*, *33*, 157–172, 1981.

Epstein, S., and T. Mayeda, Variation of O^{18} content of waters from natural sources, *Geochim. Cosmochim. Acta*, *4*, 213–224, 1953.

Erez, J., and B. Luz, Experimental paleotemperature equation for planktonic foraminifera, *Geochim. Cosmochim. Acta*, *47*, 1025–1031, 1983.

Fairbanks, R. G., and P. H. Wiebe, Foraminifera and chlorophyll maximum: Vertical distribution, seasonal succession, and paleoceanographic significance, *Science*, *209*, 1524–1526, 1980.

Fairbanks, R. G., C. D. Charles, and J. D. Wright, Origin of global meltwater pulses, in *Radiocarbon After Four Decades: An Interdisciplinary Perspective*, edited by R. E. Taylor, A. Long, and R. S. Kra, pp. 473–500, Springer-Verlag, New York, 1992.

Frew, R. D., K. J. Heywood, and P. F. Dennis, Oxygen isotope study of water masses in the Princess Elizabeth Trough, Antarctica, *Mar. Chem.*, *49*, 141–153, 1995.

Ganssen, G., and D. Kroon, Evidence for Red Sea surface circulation from oxygen isotopes of modern surface waters and planktonic foraminiferal tests, *Paleoceanography*, *6*, 73–82, 1991.

Gat, J. R., Oxygen and hydrogen isotopes in the hydrologic cycle, *Annu. Rev. Earth Planet. Sci.*, *24*, 225–62, 1996.

Gat, J. R., and R. Gonfiantini (Eds.), *Stable Isotope Hydrology: Deuterium and Oxygen-18 in the Water Cycle*, Int. At. Energy Agency, Vienna, 1981.

Houghton, J. T., G. J. Jenkins, and J. J. Ephraums, *Climate Change: The IPCC Scientific Assessment*, 365 pp., Cambridge Univ. Press, New York, 1990.

Jouzel, J., R. D. Koster, R. J. Suozzo, G. L. Russell, J. W. C. White, and W. S. Broecker, Simulations of HDO and $H_2{}^{18}O$ atmospheric cycles using the NASA GISS general circulation model: Sensitivity experiments for present-day conditions, *J. Geophys. Res.*, *96*, 7495–7507, 1991.

Keigwin, L. D., The Little Ice Age and Medieval Warm Period in the Sargasso Sea, *Science*, *274*, 1504–1508, 1996.

Kim, S.-T., and J. R. O'Neil, Equilibrium and nonequilibrium oxygen isotope effects in synthetic carbonates, *Geochim. Cosmochim. Acta*, *61*, 3461–3475, 1997.

Kohfeld, K. E., R. G. Fairbanks, S. L. Smith, and I. D. Walsh, *Neogloboquadrina pachyderma* (sinistral coiling) as paleoceanographic tracers in polar oceans: Evidence from Northeast Water Polynya plankton tows, sediment traps, and surface sediments, *Paleoceanography*, *11*, 679–699, 1996.

Large, W. G., J. C. McWilliams, and S. C. Doney, Oceanic vertical mixing: A review and a model with non-local boundary layer parameterization, *Rev. Geophys.*, *32*, 363–403, 1994.

Legates, D. R., and C. J. Willmott, Mean seasonal and spatial variability in gauge corrected, global precipitation, *Inter. J. Climatol.*, *10*, 111–127, 1990.

Lehmann, M., and U. Siegenthaler, Equilibrium oxygen-isotope and hydrogen-isotope fractionation between ice and water, *J. Glaciol.*, *37*, 23–26, 1991.

Levitus, S., R. Burgett, and T. P. Boyer, World ocean atlas 1994, Technical report, U.S. Dep. of Comm., Washington, D.C., 1994.

Lohmann, G. P., A model for variation in the chemistry of planktonic foraminifera due to secondary calcification and selective dissolution, *Paleoceanography*, *10*, 445–458, 1995.

Macdonald, R. W., D. W. Paton, E. C. Carmack, and A. Omstedt, The freshwater budget and under-ice spreading of Mackenzie River water in the Canadian Beaufort Sea based on salinity and $^{18}O/^{16}O$ measurements in water and ice, *J. Geophys. Res.*, *100*, 895–919, 1995.

Majoube, M., Fractionment en oxygène-18 et en deuterium entre l'eau et sa vapeur, *J. Chim. Phys.*, *10*, 1423–1436, 1971.

Merlivat, L., and J. Jouzel, Global climatic interpretation of the deuterium-oxygen 18 relationship for precipitation, *J. Geophys. Res.*, *84*, 5029–5033, 1979.

Milliman, J. D., and R. H. Meade, World-wide delivery of river sediment to the oceans, *J. Geol.*, *91*, 1–21, 1983.

Mix, A. C., The oxygen-isotope record of glaciation, in *The Geology of North America*, vol. K–3, *North America and Adjacent Oceans During the Last Deglaciation*, edited by W. F. Ruddiman and H. E. Wright, chap. 6, pp. 111–135, Geol. Soc. of Am., Boulder, Colo., 1987.

Mook, W. G., The oxygen-18 content of rivers, *SCOPE*, *52*, 565–570, 1982.

Mulitza, S. M., T. Wolff, J. Pätzold, W. Hale, and G. Wefer, Temperature sensitivity of planktic foraminifera and its influence on the oxygen isotope record, *Mar. Micropaleontology*, *33*, 223–240, 1998.

Oort, A. H., Global atmospheric circulation statistics, 1958–1973, NOAA Prof. Pap., *14*, 180 pp., 1983.

Östlund, H. G., and G. Hut, Arctic Ocean water mass balance from isotope data, *J. Geophys. Res.*, *89*, 6373–6381, 1984.

Östlund, H. G., H. Craig, W. S. Broecker, and D. Spenser, GEOSECS Atlantic, Pacific and Indian Ocean expeditions: Shorebased Data and Graphics, vol. 7, Technical report, Natl. Sci. Found., Washington, D.C., 1987.

Rohling, E. J., and G. R. Bigg, Paleosalinity and $\delta^{18}O$: A critical assessment, *J. Geophys. Res.*, *103*, 1307–1318, 1998.

Rossow, W. B., and Y.-C. Zhang, Calculation of surface and top-of-atmosphere radiative fluxes from physical quantities based on ISCCP datasets, 2, Validation and first results, *J. Geophys. Res.*, *100*, 1167–1197, 1995.

Rostek, F., G. Ruhland, F. C. Bassinot, P. J. Müller, L. D. Labeyrie, Y. Lancelot, and E. Bard, Reconstructing sea surface temperature and salinity using $\delta^{18}O$ and alkenone records, *Nature*, *364*, 319–321, 1993.

Rozanski, K., L. Araguás-Araguás, and R. Gonfiantini, Isotopic patterns in modern global precipitation, in *Climate Change in Continental Isotopic Records*, *Geophys. Monogr. Ser.*, 78, edited by P. K. Swart et al., AGU, Washington, D.C., 1993.

Russell, G. L., J. R. Miller, and D. H. Rind, A coupled atmosphere-ocean model for transient climate change, *Atmos. Ocean*, *33*, 683–730, 1995.

Sautter, L. R., and R. C. Thunell, Seasonal succession of planktonic foraminifera: Results from a four year time-series sediment trap experiment in the northeast Pacific, *J. Foraminiferal Res.*, *19*, 253–267, 1989.

Schmidt, G. A., Oxygen-18 variations in a global ocean model, *Geophys. Res. Lett.*, *25*, 1201–1204, 1998.

Schmidt, G. A., Error analysis of paleosalinity calculations, *Paleoceanography*, *14*, 422–429, 1999.

Shackleton, N. J., Oxygen isotope analyses and Pleistocene temperatures, reassessed, *Nature*, *215*, 15–17, 1967.

Spero, H. J., J. Bijma, D. W. Lea, and B. E. Bemis, Effect of seawater carbonate concentration on foraminiferal carbon and oxygen isotopes, *Nature*, *390*, 497–500, 1997.

Wajsowicz, R. C., A consistent formulation of the anisotropic stress tensor for use in models of the large-scale ocean circulation, *J. Comp. Phys.*, *105*, 333–338, 1993.

Wang, L., M. Sarnthein, J.-C. Duplessy, H. Erlenkeuser, S. Jung, and U. Pflaumann, Paleo sea-surface salinities in the low-latitude Atlantic: The $\delta^{18}O$ record of *Globigerinoides ruber* (white), *Paleoceanography*, *10*, 749–761, 1995.

Weiss, R. F., H. G. Östlund, and H. Craig, Geochemical studies of the Weddell Sea, *Deep Sea Res., Part A*, *26*, 1093–1120, 1979.

Wellington, G. M., R. B. Dunbar, and G. Merlen, Calibration of stable oxygen isotope signatures in Gálapagos corals, *Paleoceanography*, *11*, 467–480, 1996.

Williams, D. F., A. W. H. Bé, and R. G. Fairbanks, Seasonal isotopic variations in living planktonic foraminifera from Bermuda plankton tows, *Palaeogeogr. Palaeoclimatol. Palaeoecol.*, *33*, 71–102, 1981.

Zahn, R., T. F. Pedersen, B. D. Bornhold, and A. C. Mix, Water mass conversion in the glacial subarctic Pacific (54°N, 148°W): Physical constraints and the benthic planktonic stable isotope record, *Paleoceanography*, *6*, 543–560, 1991.

G. A. Schmidt, NASA Goddard Institute for Space Studies and Center for Climate Systems Research, Columbia University, 2880 Broadway, New York, NY 10025. (gschmidt@giss.nasa.gov)

Received October 13, 1998; revised April 23, 1999; accepted April 26, 1999.

This preprint was prepared with AGU's LaTeX macros v5.01. File paper formatted May 19, 1999.